The Astronomical Journal, 159:107 (11pp), 2020 March https://doi.org/10.3847/1538-3881/ab5fe7

Mineralogical Criteria for the Parent Asteroid of the "Carbonaceous" Achondrite NWA 6704

Allison M. McGraw[1], Vishnu Reddy[1], Matthew R. M. Izawa[2], Juan A. Sanchez[3], Lucille Le Corre[4], Edward A. Cloutis[5], Daniel M. Applin[5], and Neil Pearson[4]
[1] University of Arizona, Lunar and Planetary Lab, 1629 E. University Boulevard, Tucson, AZ 85721, USA; ammcgraw@email.arizona.edu
[2] Okayama University-Misasa, 827 Yamada, Misasa, Tottori 682-0193, Japan
[3] Planetary Science Institute, 1700 East Fort Lowell, Suite 106, Tucson, AZ 85719-2395, USA
[4] Planetary Science Institute, 1700 East Fort Lowell Road, Tucson, AZ 85719, USA
[5] Department of Geography, University of Winnipeg, Winnipeg MB R3B 2E9, Canada
Received 2019 October 13; revised 2019 November 29; accepted 2019 December 7; published 2020 February 13

Abstract

The unique achondrite meteorite Northwest Africa (NWA) 6704 and its paired samples are fragments of an unknown parent asteroid that experienced large-scale igneous melting early in our solar system's history. The geochemistry and mineralogy of NWA 6704 show that its parent asteroid has affinities with carbonaceous chondrites and that the precursor materials were relatively oxidized. While large-scale melting has affected the meteorite, there is no evidence for equilibration with a metallic melt. NWA 6704 paired meteorites therefore provide insights into the evolution of planetesimals and bodies that accreted from source materials, possibly in the ice-rich outer solar system. Currently, we lack an understanding of the distribution of potential parent asteroids of the NWA 6704 meteorites. We have undertaken a detailed multiwavelength (0.35–25 μm) spectroscopic and geochemical investigation of NWA 6704 to provide constraints on the potential parent asteroids of these enigmatic meteorites. In comparison with asteroid spectra, NWA 6704 is similar to the S(VI) subtypes of the S-asteroid complex. By using the Bus-DeMeo Taxonomic Classifier, we determine that NWA 6704 has affinities toward V-type (Vesta type) asteroids. We have determined that the parent asteroid of NWA 6704 would be a V-type asteroid that is not dynamically linked to Vesta and also fall in the S(VI) subtype of the Band I center versus Band area ratio diagram. A search in the literature for potential parent bodies yielded one asteroid, (34698) 2001 OD22, as a possible candidate.

Unified Astronomy Thesaurus concepts: Asteroid belt (70); Asteroids (72); Main belt asteroids (2036); Achondrites (15); Meteorites (1038); Infrared astronomy (786); Infrared telescopes (794); Spectroscopy (1558)

1. Introduction

Meteorites are the only bulk materials from their parent asteroids available for study on Earth. They help us constrain the compositional makeup and understand the geological history of the solar system. Many meteorites, however, lack context because we do not know the parent bodies (or class of solar system objects) from which they originated. Without context, it is challenging to address the questions about the origin and evolution of these bodies over the course of the solar system's history. Linking them to plausible parent asteroid bodies is therefore a major goal in planetary science. Reflectance spectroscopy of well-characterized meteorite samples is one of the cornerstones of this effort (e.g., Gaffey et al. 1993; Cloutis 2002; Cloutis et al. 2016). In this study, we have undertaken a mineralogical, spectroscopic, and geochemical study of the uniquely oxidized "carbonaceous" achondrite Northwest Africa 6704 (NWA 6704), with the aim of constraining its possible parent bodies in the asteroid belt.

Achondrite meteorites are defined by a lack or deficiency of chondrules and are dominated by silicate mineral assemblages. According to the current classification of meteorites (Weisberg et al. 2006), achondrites are considered to be either "primitive" or "differentiated," and contain discrete clans and groups within each. The differentiated achondrites represent silicate material that has undergone differentiation processes, while the primitive achondrites are differentiated to a much lesser degree. In addition, Weisberg et al. (2006) offer an alternative interpretive scheme for meteorite classification that utilizes oxygen isotopic reservoirs. Stable isotope analyses reveal that meteorites are grouped according to the reservoirs from which they formed, and show that currently analyzed planetary materials fall into two large groups, which may be termed "carbonaceous" and "noncarbonaceous" (e.g., Warren et al. 2013). Only a few achondrites have isotopic affinities associated with the "carbonaceous" reservoir of the solar system materials, but they offer unique insights into geological processes in large, carbonaceous bodies. The anomalous/ungrouped achondrites are a rare subgroup of differentiated achondrites comprising 84 known specimens, accounting for 3% of the terrestrial achondrite collection (The Meteoritical Bulletin). Though this is a small fraction of the total achondrite collection, the geochemical inspiration to find their parent bodies lies within the nature of their highly oxidized protoliths and carbonaceous-like isotopic measurements coexisting with their silicate mineralogy.

Most of the known achondrites (~75%) are Howardites, Eucrites, and Diogenites (HEDs). The HEDs have been compositionally linked to asteroid (4) Vesta as their parent asteroid source (McCord et al. 1970; Larsen & Fink 1975; Drake 1979; Binzel & Xu 1993; Gaffey 1997; Sunshine et al. 2004; Mayne et al. 2009; Reddy et al. 2015), where eucrites represent the crustal material of Vesta, diogenites represent the deeper crustal material, and howardites represent the regolith mixture between eucrites and diogenites (McSween et al. 2013). Though this linkage has been confirmed through spectroscopic and geochemical techniques, there is still much

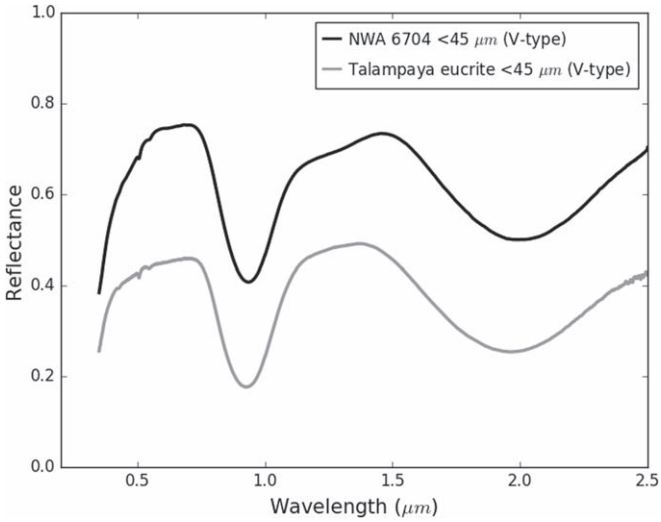

Figure 1. Visible and near-infrared spectra (0.35–2.5 μm) of anomalous achondrite NWA 6704 and Talampaya eucrite (grain size <45 μm). Near ~1 and ~2 μm, these achondrite meteorites appear spectrally similar, due to the similar silicate mineralogy. Spectra are offset by 0.1 for visual clarity. Both spectra are classified as V types under the Bus-DeMeo taxonomic system (DeMeo et al. 2009), suggesting that taxonomy alone is not a diagnostic to differentiate between HEDs and anomalous achondrites.

Figure 2. Photograph of anomalous achondrite NWA 6704 showing igneous cumulate texture with millimeter-sized grains. Scale is 1 cm in length. NWA 6704 is dominated by an Fe-rich pyroxene.

work to be done as it stands as one of the few confirmed linkages. It has been estimated that the terrestrial meteorite collection samples at least ~110 different parent bodies, 35 of which belong to the achondrite meteorite classification (Greenwood et al. 2017). The success of the linkages between HEDs and asteroid (4) Vesta provides great insight into small-body differentiation processes and confirms techniques using reflectance spectroscopy as diagnostic tools for meteorite and asteroid linkages.

The use of reflectance spectroscopy as a diagnostic tool in the visible and near-infrared (VNIR) wavelengths (0.35–2.5 μm) has shown limitations when applied to finding non-HED parent bodies. The anomalous achondrites appear spectrally similar to HEDs in the VNIR wavelength range (0.35–2.5 μm), because they share similar silicate mineralogy, making their spectra degenerate. This is especially true for studies that involve the use of spectral curve matching and taxonomic classification of asteroid and meteorite spectra, which are unable to distinguish between HED meteorites and anomalous achondrites. For example, both achondrite meteorite types shown in Figure 1 were classified as V-type asteroids (Vesta-like) by the Bus-DeMeo taxonomic classification system (DeMeo et al. 2009). However, several anomalous achondrites differ in oxygen, chromium, and titanium isotope ratios, requiring an origin from an oxidized parent bodies other than asteroid (4) Vesta. These variations in stable isotopes that are evident among the anomalous achondrites further reinforce the distinction from the HEDs (Greenwood et al. 2017). Previous work has determined a subset of the achondrites with anomalous oxygen isotope values which includes the following: Ibitira (eucrite) and NWA 011 (ungrouped achondrite; Yamaguchi et al. 2002), Pasamonte (eucrite; Weichert et al. 2004; Greenwood et al. 2005; Scott et al. 2009), Emmaville (eucrite; Greenwood et al. 2013), Asuka 881394 (eucrite; Scott et al. 2009), and Bunburra Rockhole (eucrite; Bland et al. 2009; Benedix et al. 2017). The oxygen isotopic diversity exposes variations in oxidizing environments on corresponding parent objects, and these variations among the sampled anomalous achondrites could be in turn revealing a suite of parental sources in the solar system.

The achondrite meteorite NWA 6704 was found in Algeria in 2010 and was subsequently classified as an anomalous achondrite meteorite (Irving & Kuehner 2011). A total of 42 pieces were recovered, and most were purchased by Greg Hupé in 2011 February. A 12.25 g sample was obtained by the University of Arizona's Lunar & Planetary Laboratory, and a portion of the sample is shown in Figure 2. This meteorite displays a striking greenish-yellow coloration, and it is relatively unaltered with regard to terrestrial weathering (hand specimen weathering grade A; petrographic weathering scale approximately W1, with minor staining of some silicates by ferric oxyhydroxides). NWA 6704 and its paired meteorites (NWA 6693, NWA 6926), along with the likely related (or paired) NWA 10132 are samples of a unique, oxidized achondrite object (e.g., Warren et al. 2013). These meteorites are dominated (~70% vol.) by 1.3 millimeter-scale crystals of low-Ca, Fe-rich pyroxene, ferrosilite, ($Fs_{41.6–42.4}$), with lesser amounts of ferroan pigeonite, Ni-bearing ferroan olivine (~12% vol.), Na-rich plagioclase feldspar, and a variety of minor and trace phases including K-feldspar, chromite ($FeCr_2O_4$), awaruite ($Ni_{2–3}Fe$), merrillite ($Ca_9NaMg(PO_4)_7$), and Ni-bearing sulfides such as heazlewoodite (Ni_3S_2) and pentlandite ($(Fe, Ni)_9S_8$; Irving et al. 2011; Warren et al. 2013). The NWA 6704 group meteorites show little evidence for equilibration with a metallic iron melt (Warren et al. 2013), yet they have undergone extensive melting (Irving et al. 2011; Jambon et al. 2012).

The materials present in NWA 6704 appear to be of basaltic nature, with evidence for ancient crystallization ages. The texture, geochemistry, and mineralogy of the NWA 6704 meteorite group were initially interpreted as an igneous cumulate melt origin (Irving et al. 2011; Jambon et al. 2012; Warren et al. 2013; Archer 2017). More recently, Hibiya et al. (2019) concluded that the NWA 6704 meteorites formed from a superheated melt, which either favors an impact-melt origin or a not fully differentiated asteroid process. Based on Pb–Pb dating, the crystallization age of NWA 6704 was determined to be 4.56280 ± 0.00046 Ga (Iizuka et al. 2013) and 4.56238 ± 0.00049 Ga (Koefoed 2017). The Pb–Pb ages overlap within the error of the Ar–Ar age of 4.56 ± 0.29 Ga determined by Fernandes et al. (2013). Amelin et al. (2019)

also reported a resetting at 4.199 ± 0.032 Ga based on the Ar–Ar chronometer, which is consistent with fluid-loss evidence from bubble trains found in the pyroxene crystals, implying rapid postcrystallization thermal metamorphism. The ancient age of NWA 6704 requires accretion and subsequent melting of an asteroid with the isotopic signature of the "carbonaceous" solar system reservoir within 3.6 Ma of the first nebular condensates forming, namely calcium aluminum inclusions (Amelin et al. 2019). The extensive melting to produce the NWA 6704 meteorites requires either the presence of significant internal radiogenic sources (i.e., ^{238}U, ^{235}U, ^{232}Th, ^{40}K, ^{26}Al, or ^{60}Fe), or a dynamical environment where highly energetic impacts could occur. Such rapid accretion may, however, be at odds with expectations of slower accretion at larger heliocentric distances. Near-chondritic values represented in the highly siderophile elements and rare-earth elements also suggest that the parental melt or protolith material that the NWA 6704 meteorite group is derived from did not experience differentiation processes (Hibiya et al. 2019). This would include separation of silicate, metal, and sulfide material, and perhaps rapid cooling after being extremely heated (as demonstrated by the volatile depletions) with no time allowance for magmatic differentiation to proceed (Hibiya et al. 2019). Whether the NWA 6704 group is impact melts or the result of endogenic igneous processes, they are at present the only samples of their parent object and are unique among known meteorites.

Stable oxygen isotope measurements have long been used to identify source reservoirs for planetary materials (e.g., Clayton et al. 1976; Clayton 1993; Clayton & Mayeda 1996, 1999). More recently, other stable isotopic systems have been applied to this problem, notably Cr, but also Ti, Ni, and others. Together, Cr, Ti, and O isotopes reveal a fundamental dichotomy in the solar system materials as represented by meteorites: one group contains the ordinary and enstatite chondrites, the Earth–Moon system, the HED parent body (4) Vesta, Mars, angrites, and ureilites (among others), and appears to represent materials accreting in the inner solar system (e.g., Warren et al. 2013). The other group is dominated by carbonaceous chondrites and is thought to reflect accretion beyond the ice line, that is, at sufficient heliocentric distances where abundant water ice condensed. There is very little evidence for mixing between these reservoirs during the accretion process (clearly, later mixing must have occurred as demonstrated by the common presence of carbonaceous chondrites in the inner solar system), apart from some chondrules in CV chondrites (Olsen et al. 2016). Among the carbonaceous group, however, are a few meteorites that reflect large-scale melting. The NWA 6704 pairing group carries Cr, Ti, and Ni isotopic signatures that link it with the carbonaceous chondrite reservoir (e.g., Warren et al. 2013). Other authors have also noted isotopic affinities of the NWA 6704 meteorite pairing group toward the carbonaceous chondrite reservoir (e.g., Hibiya et al. 2019; Sanborn et al. 2019). Denoting NWA 6704 and its pairing group as a "carbonaceous" achondrite is reasonable given isotopic affinities and accretionary parentage of these meteorites.

The Δ^{17}O and ε^{54}Cr signatures of the solar system materials show a bimodal distribution (Figure 3; e.g., Warren 2011; Sanborn et al. 2019). NWA 6704 and its paired meteorites fall among the carbonaceous chondrite distribution in the Δ^{17}O space, which promotes giving them the title "carbonaceous"

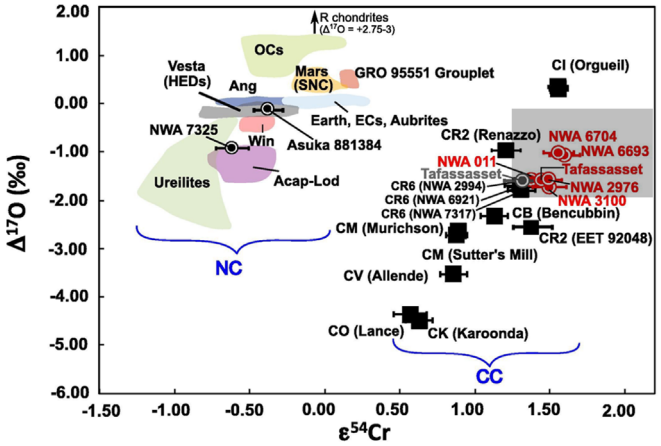

Figure 3. ^{17}O vs. ^{54}Cr plot from Sanborn et al. (2019) showing the bimodal distribution of noncarbonaceous (NC) and carbonaceous (CC) materials from the solar system. NWA 6704 and paired meteorites are highlighted in the gray box. NWA 6704 and paired meteorites NWA 6693 and NWA 011 are consistent with that of the carbonaceous material distribution. Denoting these achondrites as "carbonaceous" achondrites could serve as a better diagnostic term.

achondrites. The isotopic bimodality of solar system materials indicates a corresponding separation of accreting material into two regions that did not exchange material for an extended period of time. Based on geochemical and mineralogical constraints, it appears that the carbonaceous-related reservoir sampled larger heliocentric distances. Nevertheless, many carbonaceous meteorites are among the terrestrial collection, and clasts of carbonaceous material are known from many inner solar system materials, indicating that the separation of the noncarbonaceous and carbonaceous reservoirs did not persist to the present day.

In summary, the "carbonaceous" achondrite meteorite NWA 6704 and its pairing group represent igneous material from an asteroid with isotopic characteristics suggesting a link with carbonaceous chondrites, and geochemical signatures of a highly oxidized protolith. Currently, there are no known candidate parent asteroids for the NWA 6704 group. Linking NWA 6704 with potential parent asteroids is an important step toward identifying this oxidized precursor reservoir. Given the limitations of existing asteroid taxonomic tools in identifying meteorite parent bodies in the VNIR wavelengths (see Figure 1), we employ diagnostic spectral band parameters to help identify the asteroid parent body of NWA 6704. In addition, we explore an extended wavelength range (2.5–25 μm) beyond the VNIR (0.35–2.5 μm) to search for additional diagnostic features which would differentiate the anomalous achondrite parent bodies from Vesta and Vestoids (the HED parent body; Figure 4). The present study takes a collaborative approach using geochemical (X-ray diffraction, XRD) and spectroscopic techniques (visible, near-infrared, and mid-infrared) to constrain and help identify possible parent asteroids of the "carbonaceous" achondrite meteorite NWA 6704.

2. Samples and Methods

2.1.1. Sample Preparation (X-Ray Diffraction)

Fragments of NWA 6704 lacking visible fusion crust or weathering materials were broken up and ground by hand with an agate mortar and pestle. The powder was dry-sieved to

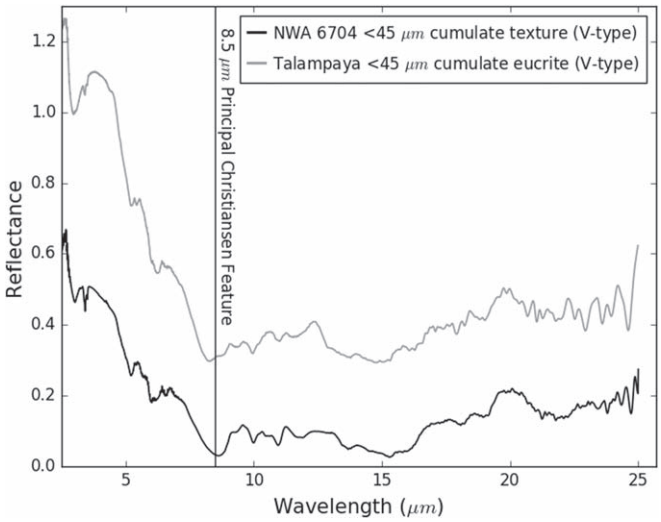

Figure 4. Mid-infrared reflectance spectra (2.5–25 μm) of the anomalous achondrite NWA 6704 and Talampaya eucrite (grain size <45 μm). The principal Christiansen feature (reststrahlen band) is shown at 8.5 μm; the band center for NWA 6704 is 8.504 and for Talampaya is 8.354 μm. Talampaya was chosen for this comparison because it is representative of coarse-textured cumulate eucrites and was recovered soon after the fall event and therefore exhibits minimal terrestrial alteration. Talampaya and NWA 6704 have similar pyroxene chemistry (Talampaya $En_{58.6–60.0}Wo_{1.2–1.6}$ vs. NWA 6704 $En_{57.6–59.4}Wo_{2.8–3.6}$) and contain a similar assemblage of ferroan pyroxene and plagioclase. The spectral differences between Talampaya are mainly due to the differing modal abundances of plagioclase: ~65% in Talampaya (Cloutis et al. 2013) vs. 14.1% in NWA 6704 (this study). The spectra are offset by 0.25 (*y*-axis) for visual clarity.

<250 μm and <45 μm fractions. The <45 μm fraction was used for XRD studies. Synchrotron powder XRD data were collected at beamline I–11, Diamond Light Source (Thompson et al. 2009), using monochromatic radiation ($\lambda = 0.824883$ Å) from 0°.001 to 150° 2θ with an effective step size of 0°.001. Powdered samples were loaded in borosilicate glass capillaries with internal diameter 400 μm. The capillaries were rotated at 120 revolutions/minute to reduce any heterogeneity or preferred orientation effects. Diffracted X-rays were collected with a multianalyzer crystal system (Thompson et al. 2009). Diffraction patterns were analyzed using the Bruker AXS EVA and QualX2 (Altomare et al. 2015) software packages and the Crystallography Open Database (Grazulis et al. 2009). Additional powder XRD patterns for NWA 6704 were collected using a Bruker D8 Discover diffractometer using Co $K\alpha_{1,2}$ radiation ($\lambda = 1.78897$ Å), accelerating voltage 40 kV, and a 40 mA beam current. A 0°.02 divergence slit was placed on the detector side of the diffractometer. XRD patterns were collected for both size fractions of each lithology with a step size of 0°.0076 and counting times of 25 s per step covering 15°–82° 2θ.

2.1.2. Methodology (Rietveld Refinement)

Rietveld refinement of XRD patterns was performed using the Bruker AXS TOPAS version 4.2 software package. Rietveld refinement uses a numerical model of a diffraction experiment, including the incident radiation, the instrument, and the structure and composition of the scattering matter to create a simulated diffraction pattern (Rietveld 1969; Young et al. 1977; Young 1993; Shankland 2004). The simulated diffraction pattern is then compared with the measured diffractogram for that sample, and nonlinear least-squares optimization of the model parameters (instrumental parameters, abundances, and crystallographic parameters of the mineral(s) present) is carried out to find the best fit of the model parameters to the diffractogram (Rietveld 1969; Young et al. 1977; Young 1993; Shankland 2004). Rietveld refinement is capable of accurately quantifying the modal mineralogy of complex mixtures (e.g., Bish & Post 1993; Gualtieri 2000; Shankland 2004; Wilson et al. 2006). Starting structural models were created using published crystal structures as follows: pigeonite—Morimoto & Güven (1970), orthopyroxene—Hugh-Jones & Angel (1994), olivine—Smyth & Hazen (1973), chromite—Lenaz et al. (2004), heazlewoodite—Fleet (1977), and pentlandite—Hall & Stewart (1973). The plagioclase model was modified from that of Fitz Gerald et al. (1986), and the awaruite model was adapted from the kamacite (α-iron) structure of Wilburn & Bassett (1978). The refinements were carried out using the fundamental parameters mode, which uses a first-principles approach to calculate the shapes and intensities of diffracted peaks, rather than a conventional fit function (e.g., pseudo-Voight profiles).

2.2.1. Sample Preparation (VNIR Spectroscopy 0.35–2.5 μm)

For the whole rock chip spectra, we used a ~5 mm wide spot on the roughened saw-cut face of the meteorite. Subsequently, a portion of the sample (~0.5 g) was removed from the slab and ground in an alumina mortar and pestle and dry-sieved to produce a <150 μm powder as well as a <45 μm powder for spectral measurements.

2.2.2. Methodology (VNIR Spectroscopy)

VNIR reflectance spectra were acquired with an ASD Field Spec Pro HR spectrometer, and sample illumination was provided by a collimated 100 W quartz–tungsten–halogen light source with a viewing geometry of $i = 30°$ and $e = 0°$. Spectra were measured relative to a calibrated Spectralon® standard and corrected for minor irregularities in Spectralon's reflectance in the >2 μm region, and occasional minor offsets at 1.00 and 1.83 μm, where detector changeovers occur. Spectral resolution varies between ~2 and 7 nm, and data are acquired at 1.4 nm intervals, which are then internally resampled by the spectrometer to provide output data at 1 nm intervals. A total of 200 spectra of the standard, dark current, and sample were acquired to improve signal to noise.

Diagnostic spectral band parameters including the band depths, band centers, and band areas of absorption features of interest were measured from the reflectance spectra using protocols described in Sanchez et al. (2012). Diagnostic band parameters from asteroid telescopic spectra were measured using the same protocols. Each spectrum is divided by a straight line continua tangent to either side of an absorption feature of interest. For the 2 μm region absorption band, the long wavelength side of the continuum was fixed at 2.5 μm. After removing the continuum, Band centers are calculated by fitting an *n*-order polynomial over the bottom third of each absorption band. Band areas are calculated using trapezoidal numerical integration and are used to calculate the Band Area Ratio (BAR), which is given by the ratio of the area of Band II to that of Band I. Band depths are measured from the continuum to the band center (Clark & Roush 1984).

Table 1
Mineral Abundances from Rietveld Refinement

Mineral	wt.%	Error	R_{Bragg}	Density	vol.%	Error
pigeonite	13.4	0.3	3.213	3.649	11.7	0.3
orthopyroxene	57.4	0.4	3.205	3.132	58.6	0.4
albite	14.1	0.4	2.938	2.619	17.2	0.5
olivine	14.4	0.2	2.559	3.860	11.9	0.2
chromite	0.8	0.4	1.439	4.950	0.5	0.3
awaruite	<0.01	n.d.	n.d.	8.358	0.004	n.d.
merrillite	<0.01	n.d.	n.d.	3.100	0.010	n.d.
pentlandite	<0.01	n.d.	n.d.	4.800	0.007	n.d.
heazlewoodite	<0.01	n.d.	n.d.	5.820	0.005	n.d.

2.3.1. Sample Preparation (MIR Spectroscopy 2.5–25 μm)

A total of 0.21 g was taken from a 12.2 g whole rock sample of NWA 6704 for the mid-infrared measurements. The material was crushed and dry-sieved by hand to a <45 μm powder using a ceramic mortar and pestle under clean conditions. The 0.21 g of NWA 6704 was placed inside of a clean aluminum sample cup for the spectral measurement.

2.3.2. Methodology (MIR Spectroscopy)

Mid-infrared (MIR) diffuse reflectance spectral data (2.5–25 μm) were collected with a Nicolet iS50R Fourier Transform InfraRed (FTIR) spectrometer at the University of Arizona at the Lunar and Planetary Laboratory. The viewing geometry of the SpecAc reflectance accessory was set to $i = 0°$, $e = 30°$, and a phase angle of 30°. Two InFraRed™ detectors were used to cover the entire MIR wavelength range: (1) the MCT D* (Mercury Cadmium Telluride) detector (2.5–12 μm), and (2) the DLaTGS (Deuterated L-alanine doped Triglycine Sulfate) detector (12–25 μm). The MCT D* detector is cryogenically cooled, and the DLaTGS is thermal electrically cooled. The MIR light source (1–25 μm) was an external Oriel Instruments MIR tungsten glowbar, where the MIR light passed through a KBr window into the FTIR spectrometer system. The MIR light also passed through a KBr beamsplitter (1.35–28.57 μm) before interacting with the meteorite sample, and then onto the detectors located inside of the FTIR system. A dry nitrogen purging technique was used in order to reduce the amount of atmospheric CO_2 and H_2O during the spectral measurements.

A total of 1500 scans were collected during the spectral measurements for both NWA 6704 and the background reference material. A diffuse aluminum disk, ground using #600 loose grit and coated with gold, was used as the background reference material for the experiment, and the FTIR software, OMNIC, completes the subtraction and Fourier transform, which yields the final reflectance spectrum from the sample.

3. Results

3.1. Results (XRD)

Mineral abundances for each phase are reported in Table 1. The errors reported in the Rietveld refinement are derived from least-squares fitting and may underestimate the true errors. The low abundance phases, chromite, awaruite, pentlandite, heazlewoodite, and merrillite are close to the detection limit of XRD. Figure 5 shows the most abundant minerals present in NWA 6704: pigeonite (pyroxene), ferrosilite (low-calcium pyroxene or LCP), fayalite (olivine), albite, awaruite, and chromite. The weighted profile residual (R_{wp}) of the Rietveld fit is 9.91%, and although there is no rigorous standard for the maximum R_{wp} that constitutes an acceptable fit, an R_{wp} value of ⩽10% is considered reasonable by many authors (Bish & Post 1993; Young 1993; Gualtieri 2000; Shankland 2004; Pecharsky & Zavalij 2005).

3.2. Results (VNIR Spectroscopy 0.35–2.5 μm)

Reflectance spectra of the rough (nonspecular) face of the whole rock chip, <150 μm and <45 μm powders are shown in Figure 6. All spectra exhibit similar properties: a rise in reflectance to a peak near 0.6 μm, an absorption feature located near 0.95 μm (Band I), a local reflectance maximum near 1.4 μm, and a second major absorption feature near 2.0 μm (Band II).

The spectral properties of the sample are consistent with its mineralogy (derived from this meteorite and paired samples): ∼70 wt.% pyroxene and 12 wt.% olivine (Irving et al. 2011; Garvie 2012; Warren et al. 2013; this study). The other major phase, albite (∼16 wt.%), is not expected to contribute any well-defined absorption features to the VNIR spectrum, but may increase overall reflectance (Nash & Conel 1974). One of the notable features of the reflectance spectra of slabs and coarse powders of NWA 6704 is the overall blue slope, with reflectance declining from the peak near 0.7 μm to the interband maximum near 1.4 μm and beyond. This is unusual among terrestrial and synthetic pyroxenes and many differentiated pyroxene-rich meteorites, such as HEDs and Martian meteorites (e.g., Adams 1974; Gaffey 1976; Cloutis & Gaffey 1991; McFadden & Cline 2005; Klima et al. 2007, 2008), where the ratio of the 0.7–1.4 μm reflectance peaks is ∼1 or less (it is 1.25 and 1.63 for the powder and chip, respectively). The steeper overall blue slope of the chip as compared to the powder is often seen in whole rock versus powder spectra, due to increased specular reflectance at short wavelengths (e.g., Pompilio et al. 2007). With increasing Fe^{2+} content, more of this cation will partition into the M1 crystallographic site, leading to an increasingly apparent absorption band near 1.2 μm (Klima et al. 2008). The presence of M1-sited Fe^{2+} is evidenced from an absorption feature that appears as a change in slope in this region (Figure 6).

The presence of low-calcium Fe^{2+}-bearing pyroxene is further supported by absorption bands located near 0.506 and 0.545 μm, both of which are attributable to spin-forbidden transitions in Fe^{2+} located in the M1 crystallographic site (Cloutis 2002; Klima et al. 2007; Figure 7). These absorption features are only present in LCP spectra and not in high-calcium pyroxene spectra (Cloutis 2002). A spectral contribution from olivine (fayalite) based on minor absorption bands is less certain. The most prominent olivine-associated absorption band is a broad feature near 0.62 μm, which has been attributed to crystal field transitions in Ni^{2+} (King & Ridley 1987), but this assignment is uncertain (Sunshine & Pieters 1998).

Previous studies (e.g., Cloutis et al. 1986; Cloutis & Gaffey 1991) have shown that the major absorption bands in the 1 and 2 μm regions, termed Band I and Band II, respectively, can be used to constrain the composition and end-member abundances for olivine + pyroxene mixtures. This analysis is based largely on the use of the wavelength positions and areas of Bands I and II (Table 2). The olivine:pyroxene

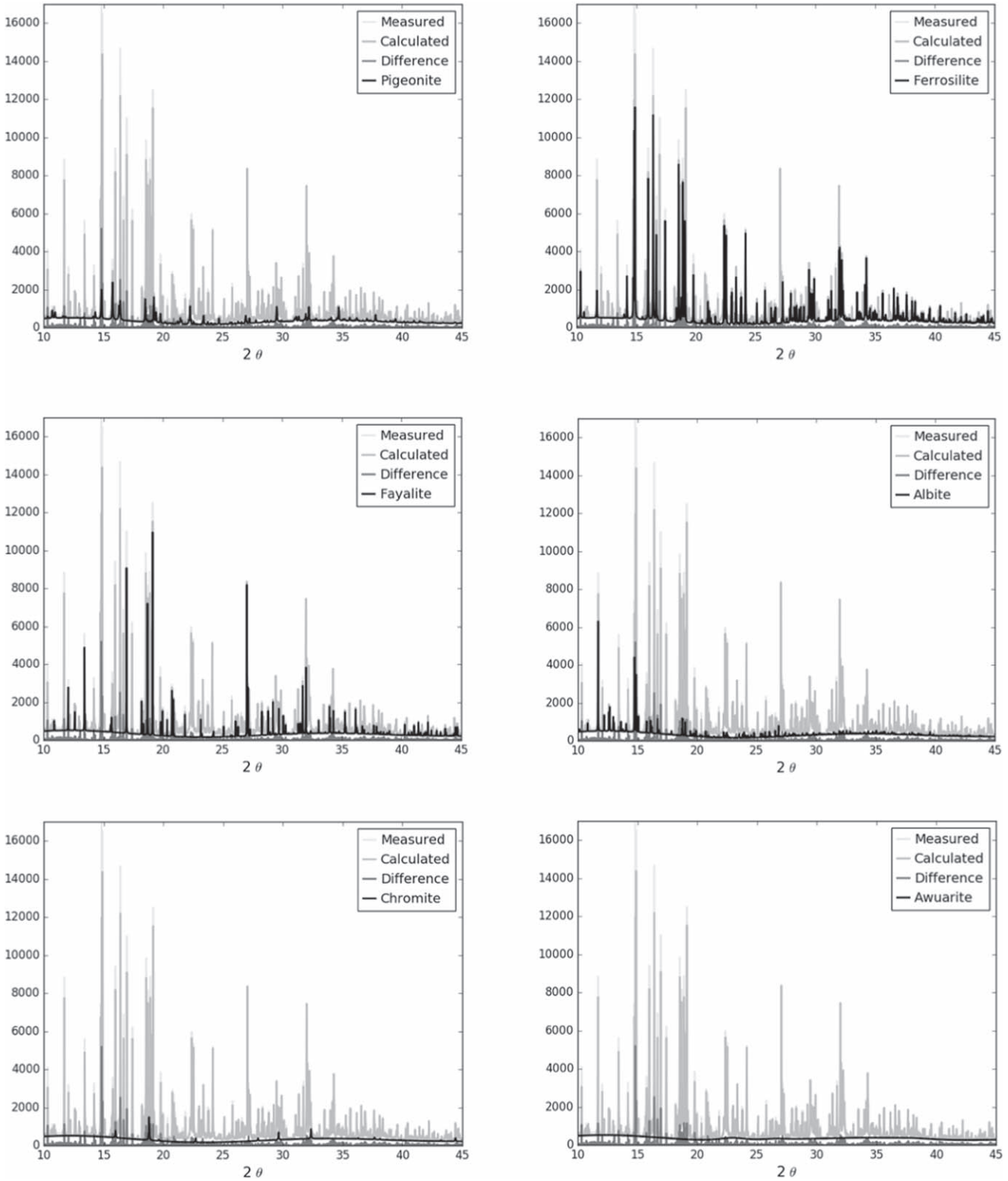

Figure 5. X-ray diffraction and Reitveld refinement shown for select minerals present in NWA 6704. Pattern matching reveals the presence of orthopyroxene, fayalitic olivine, pigeonite, chromite, albite, merrillite, awaruite, heazlewoodite, and pentlandite. The Rietveld refinement fit shows a qualitatively "good" visual match, with weighted profile residual ($R_{wp} = 9.91$). Individual abundances and R_{Bragg} values for each refined phase are given in Table 1.

ratio is usually determined from the ratio of the Band II/Band I areas (termed the Band area ratio, or BAR; Cloutis et al. 1986), and it increases with increasing pyroxene:olivine ratio, because pyroxene has absorption features in the 1 and 2 μm regions (Band I and Band II), while olivine only has an absorption feature in the 1 μm region (Band I). The BAR of NWA 6704 varies between 1.16 and 1.36 for the powders and to 1.32 for the chip (Table 2). The variation presented here in the powders and the chip is likely due to particle size effects (Harloff & Arnold 2001).

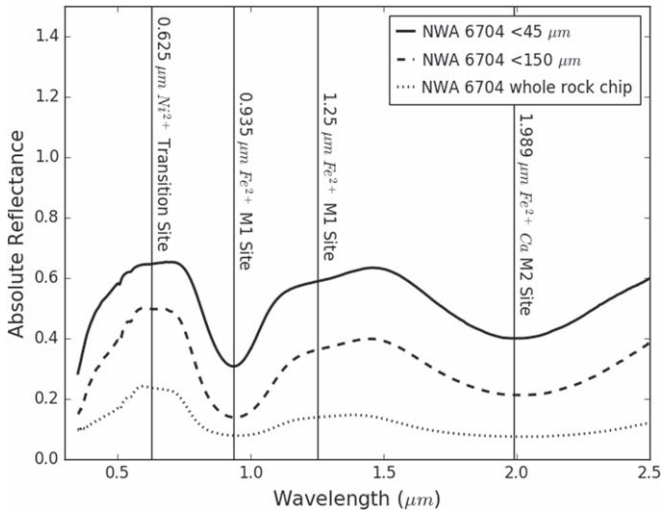

Figure 6. Visible and near-infrared spectra (0.35–2.5 μm) of the anomalous achondrite NWA 6704 for a rough (nonspecular) face of a whole rock chip, <150 μm and <45 μm crushed and sieved powders. All samples exhibit similar spectral properties: a rise in reflectance to a peak near 0.6 μm, an absorption feature located near 0.935 μm, a local reflectance maximum near 1.4 μm, and a second major absorption feature near 2.0 μm. A minor absorption feature located at 0.625 μm is also visible, and more evident as the grain size increases, due the presence of a Ni transition (Wood 1974). A minor absorption near 1.25 μm may be present from a higher content of Fe in the M1 site of the pyroxene crystals.

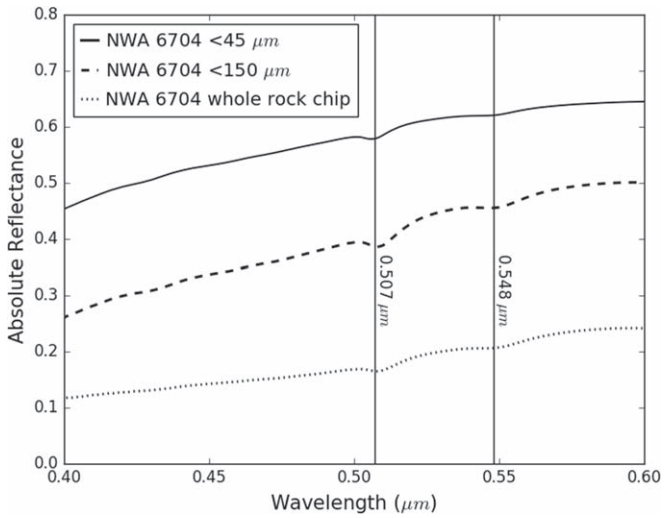

Figure 7. Visible wavelength spectra (0.4–0.6 μm) of NWA 6704 showing a minor absorption feature, due to the presence of low-calcium Fe^{2+}-bearing pyroxene, as evidenced from absorption bands located near 0.507 μm and 0.548 μm, though it is greatly lessened in depth for the <45 μm sample. These spectral features are attributable to the spin-forbidden transitions in Fe^{2+} located within the pyroxene M1 crystallographic site (Cloutis 2002; Klima et al. 2007). The steep UV dropoff is due to Fe–O charge transfer processes, consistent with an abundance of Fe-bearing minerals. Terrestrial weathering products containing Fe^{3+} also contribute to this spectral signature.

The wavelength position of Band II is a function of pyroxene composition (Fe^{2+} and Ca content) and is unaffected by the presence of olivine (Cloutis et al. 1986). The centers of the Band II parameter are 1.968 μm (whole rock chip), 2.006 μm (<150 μm powder), and 1.990 μm (<45 μm powder). Visually, it appears that Band II may be saturated in the whole rock chip spectrum (evidenced by a low reflectance and a wide, shallow minimum; Pompilio et al. 2009). Using the <45 μm powder Band II value, we calculate a pyroxene composition of $Fs_{45\pm3}$ using Burbine et al. (2018) equations, which is consistent with the XRD measurements (Table 2). Olivine composition cannot be determined very effectively for pyroxene + olivine mixtures. However, if pyroxene composition can be constrained, olivine composition can be similarly constrained if an equilibrium assemblage is assumed (e.g., Nafziger & Muan 1967).

Both Band I position and BAR are functions of pyroxene and olivine compositions and the relative abundances (Cloutis et al. 1986). These values (Table 2), when plotted relative to the regions defined by various S-type asteroid subgroups (Figure 8) suggest a pyroxene/pyroxene + olivine ratio of 0.85 (Cloutis et al. 1986). When compared to S-asteroid subgroups (Gaffey et al. 1993), the Band I center and BAR values for NWA 6704 plot close to the S(VI) subgroup. The S(VI) region is characterized by asteroids with silicate surface mineralogy where orthopyroxene is in higher abundance relative to olivine. Gaffey et al. (1993) originally categorized the S(VI) region with spectra from specific S-type asteroids: (20) Massalia, (82) Alkmene, and possibly (1036) Ganymed. However, the authors made special note that this region could be considered somewhat arbitrary as the initial band parameters derived have large error bars associated with them. Overall, the Band I center and BAR of all three grain size bins of NWA 6704 (<45 μm, <150 μm, and a whole rock chip) of this study are consistent with S(VI) subtype asteroids. It is important to note that some primitive achondrites fall within the S(VI) region of Band I center versus BAR plot (Lucas et al. 2019). However, they plot below the spectral band parameters for NWA 6704 and do not share compositional affinity.

3.3. Results (MIR Spectroscopy 2.5–25 μm)

The mid-infrared spectrum of NWA 6704 is shown in Figure 9. Overall, the spectrum shows crystal field absorption features that are consistent with mafic silicate-dominated mineralogy, which is in agreement with the XRD measurements (Figure 5). Figure 10 shows NWA 6704 reflectance spectra compared to reflectance spectra of a pure end-member synthetic pyroxene (100% Fe-rich with no Mg present) published in Klima et al. (2011). Adsorbed water and terrestrial organic contamination is evident from 2.7 to 4 μm; therefore, no analysis was performed in this wavelength region. The MIR spectrum of NWA 6704 shows the effect of particle size between the principal reststrahlen bands (beyond ~8.5 μm), where Si–O–Si bonds within silicate minerals experience stretching and bending vibrational modes (Cooper et al. 2002). As the wavelength of the source light increases toward the grain size of the sample, the volume scattering effect changes spectral minima to reflectance maxima. Hence, some absorption features in the MIR may appear as spectral maxima instead of minima.

The displacement of oxygen atoms in the Si–O bond causes asymmetrical stretching in the 8.5 to 12 μm range. This is largely due to a disturbance of the oxygen atom in the silica tetrahedral structure. NWA 6704 displays a strong absorption feature of this nature near 8.5 μm, as does the comparative pure-Fe pyroxene end-member spectra (Figure 10). The 8.5 μm absorption feature is due to vibrational asymmetrical stretching of the Si–O–Si bond. The reststrahlen band center of the principal Christiansen feature was measured to be 8.504 μm, which is consistent with similar pyroxene chemistry (Figures 4 and 10). Deformation and bending modes are typically between

Table 2
Spectral Band Parameters of Northwest Africa 6704

Band Area Ratio (BAR) for NWA 6704 Samples						
Spectral Band Parameters	<45 μm powder		<150 μm powder		Whole rock chip	
Pyroxene chemistry	Fs (mol%)	Wo (mol%)	Fs (mol%)	Wo (mol%)	Fs (mol%)	Wo (mol%)
Band I, 1 μm region	42 ± 4	9 ± 1	43 ± 4	9 ± 1	30 ± 4	5 ± 1
Band II, 2 μm region	45 ± 3	11 ± 1	49 ± 3	12 ± 1	40 ± 3	9 ± 1
Band I	0.935 ± 0.005 μm		0.935 ± 0.005 μm		0.924 ± 0.005 μm	
Band II	1.990 ± 0.007 μm		2.006 ± 0.005 μm		1.968 ± 0.005 μm	
BAR	1.365 ± 0.02 μm		1.163 ± 0.02 μm		1.320 ± 0.03 μm	

Note. Abbreviations: Fs: molar % ferrosilite; Wo: molar % wollastonite.

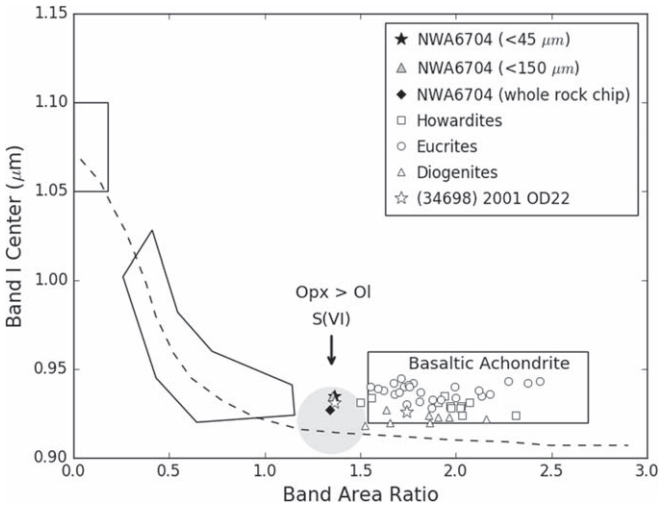

Figure 8. NWA 6704 spectral band parameters (Band I center, BAR) for three separate grain size bins measured in this study (<45 μm, <150 μm, and a whole rock chip) plotted with HED meteorites (Le Corre et al. 2015 and references therein). Two separate band parameter sets for parent asteroid candidate (34698) 2001 OD22 from Hardersen et al. (2018) are shown, one in the S(VI) region and one plotting in the Basaltic Achondrite region.

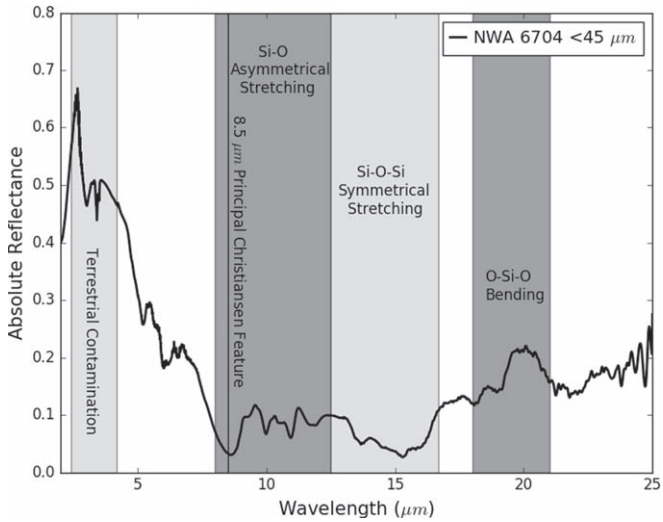

Figure 9. Mid-infrared spectrum (2.5–25 μm) of NWA 6704 showing minor absorption features due to O–H stretching mode near ~3 μm from terrestrial contamination, Si–O asymmetrical stretching motions (10.96 μm) from displacements in Si atoms, and Si–O–Si symmetrical stretching (13.6 μm). A major absorption feature coincides with the principal Christiansen feature occurring at 8.5 μm in the region between ~8–12.5 μm where reflectance minima become reflectance maxima, due to particle and volume scattering effects (Salisbury et al. 1987). Major absorption features from O–Si–O bending at 18 and 20 μm are present due to the displacement of oxygen atoms in the silica tetrahedral crystal structure; however, here the absorption features are inverted to a trough-like structure, due to strong scattering effects in longer wavelengths (Salisbury et al. 1987).

16.6 and 25 μm in the O–Si–O structure, and NWA 6704 shows this feature near 18 and 20 μm (Figure 9). Asymmetrical stretching due to displacements of Si atoms shows a minor absorption feature near 10 μm (Figure 9).

4. Discussion

In this study, our goal was to identify a parent asteroid of the anomalous achondrite NWA 6704 using diagnostic spectral band parameters. Based on what we have learned about NWA 6704, we can list the characteristics that an asteroid should meet to be considered a possible parent body for this meteorite: (1) as noted in Figure 1, spectra of HED meteorites (Talampaya eucrite) and anomalous achondrite (NWA 6704) are classified as V types under the Bus-DeMeo taxonomic system (DeMeo et al. 2009); therefore, the asteroid must be classified as a V type, but one that is not dynamically linked to Vesta and the Vesta family, because NWA 6704 does not belong to the HED clan. (2) HED meteorites and V-type asteroids related to Vesta fall into the Basaltic Achondrite (BA) region; in contrast, our analysis of the spectral band parameters (Band I center and BAR) shows that anomalous achondrites such as NWA 6704 fall in the S(VI) region of the Gaffey et al. (1993) S-asteroid subtypes. Hence, we would expect the parent body to fall in the S(VI) region as well. (3) Because the O-isotopic composition of NWA 6704 seems to link it to carbonaceous chondrites, the V-type parent body is probably located in a region mostly populated by primitive asteroids. (4) The composition of the asteroid, derived from the Band parameters, should be similar to that derived for NWA 6704 from the laboratory spectra of this study. (5) The parent body should be close to a resonance capable of transporting fragments of the Main Belt asteroid to near-Earth space.

A search in the literature for potential parent bodies shows that only a few V-type asteroids not linked to Vesta and its family have been found (e.g., Lazzaro et al. 2000; Hardersen et al. 2004; Migliorini et al. 2017; Hardersen et al. 2018). Among these objects, we have identified one asteroid, (34698) 2001 OD22, as a possible candidate (Figure 11). 2001 OD22 is an ~8 km diameter (Masiero et al. 2011) object located in the outer belt. NIR spectra (0.7–2.5 μm) obtained with NASA's Infrared Telescope Facility showed the two prominent

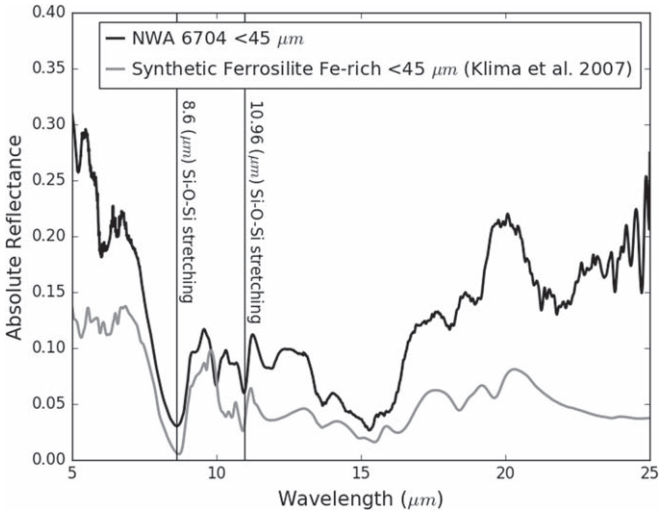

Figure 10. Mid-infrared spectra (5–25 μm) of NWA 6704 compared to a representative pure Fe-rich synthetic pyroxene end-member, ferrosilite, (Klima et al. 2007). The synthetic pyroxene mixture is 100% Fe (Mg-free). Ferrosilite spectral data obtained from Brown University Keck/NASA Relab, Spectrum number DL-CMP-061-A/BIR1DL061A.

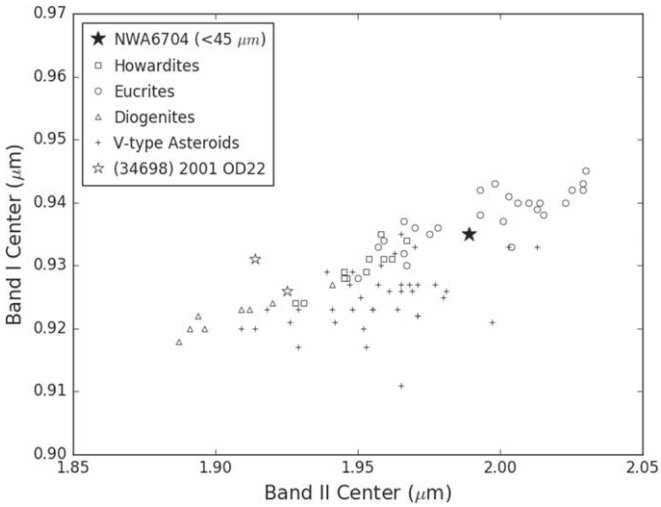

Figure 11. Band I and II centers for NWA 6704 (<45 μm), HEDs from Le Corre et al. (2015), V-type asteroids (Leith et al. 2017), and candidate parent asteroid (34698) 2001 OD22 (Hardersen et al. 2018). We used <45 μm band centers for NWA 6704 because it closely resembles the regolith present on an 8 km Main Belt asteroid. Despite NWA 6704 band centers being in closer proximity to other V types than OD22, they do not meet the other three criteria for the asteroid–meteorite linkage.

absorption bands centered at the ~0.9 and 1.9 μm characteristics of V types (Hardersen et al. 2018). This, along with its orbital parameters (a = 3.18 au, i = 23°.23, e = 0.07), makes this asteroid meet the first condition described above.

Hardersen et al. (2018) obtained two spectra of 2001 OD22 and found that when plotted in the Band I center versus BAR diagram, one spectrum was consistent with a BA analog and the other with the S(VI) subgroup (Figure 8). They suggested that the different BAR values could be the result of surface compositional variations, but indicated that additional observations would be needed to confirm their results. Because one of the spectra of 2001 OD22 falls in the S(VI) subgroup like NWA 6704 (Figure 8), we consider this asteroid to meet the second parent body condition.

The asteroid 2001 OD22 belongs to the Alauda family, a high-inclination family composed of primitive (C-complex) asteroids residing in the outer region of the Main Belt with ~1300 members (Gil-Hutton 2006; Novakovic et al. 2011; Nesvorny 2015). The primary parent body of the family, (702) Alauda, is a ~195 km diameter asteroid, which is known to have a small satellite thought to be the result of a subcatastrophic collision experienced by Alauda (Rojo & Margot 2007, 2011). The pyroxene-rich, basalt-like spectral signatures of 2001 OD22 combined with an association with carbonaceous asteroids and evidence of a large collision are all consistent with a link to NWA 6704 and its paired meteorites.

With the first three conditions met, we have to look now at the derived composition of 2001 OD22 and see whether it is similar to that of NWA 6704. Using the band centers measured by Hardersen et al. (2018), we have recalculated the pyroxene chemistry of the asteroid using the updated equations of Burbine et al. (2018). We obtained a value of $Fs_{33\pm4}$ for the asteroid, which is about 10% lower than the one derived for NWA 6704 ($Fs_{44\pm4}$). The Fs value is influenced by the position of the band centers. The Band I and II centers of 2001 OD22 were measured to be 0.931 ± 0.004 μm, and 1.914 ± 0.010 μm, respectively (Hardersen et al. 2018). The Band I center is very close to the value we measured for the <45 μm grain sample (0.935 ± 0.005 μm); however, there is a difference of ~0.08 μm between the Band II center of the asteroid and the meteorite sample (1.990 ± 0.007 μm).

Influences from temperature variations, grain size variations, and elemental composition can all affect where the center of a spectral band resides. For example, band centers are known to shift with temperature variations (e.g., Moroz et al. 2000; Hinrichs & Lucey 2002; Reddy et al. 2012), and the difference between the room temperature at which laboratory spectra are obtained and the much lower surface temperature of an asteroid in the outer belt could result in differences in the band centers. However, Hardersen et al. (2018) applied temperature corrections to the band centers of 2001 OD22 in order to account for this effect, minimizing with this the influence of temperature on these parameters. Other laboratorial spectral band parameter measurements have shown sensitivities to variations in grain sizes of powders (Harloff & Arnold 2001). Grain size variations affect the position of the band centers, for instance, we found a difference of ~0.02 μm between the Band II center of the <45 μm and the <150 μm grain size samples, and a difference of ~0.04 μm between the <150 μm grain size and the whole rock chip (Table 2). Thus, a difference in grain size between the surface regolith of the asteroid and the laboratory samples could partially explain the discrepancy.

Another important factor to consider for spectral band center locations is elemental composition of minerals. Specifically, pyroxene band centers shift to longer wavelengths as the iron or calcium content increases. For NWA 6704, we found a fraction of 13.4 wt% of pigeonite (Table 1), and the Band II center of this Ca-bearing clinopyroxene typically occurs at wavelengths >2 μm. Thus, a lower content of this mineral on the surface of the asteroid compared to the meteorite sample could explain the discrepancy in the Band II centers. As stated earlier, Hardersen et al. (2018) suggested the possibility of compositional variations across the surface of 2001 OD22, which opens the possibility that regions of the asteroid that were not observed could be closer in composition to NWA 6704.

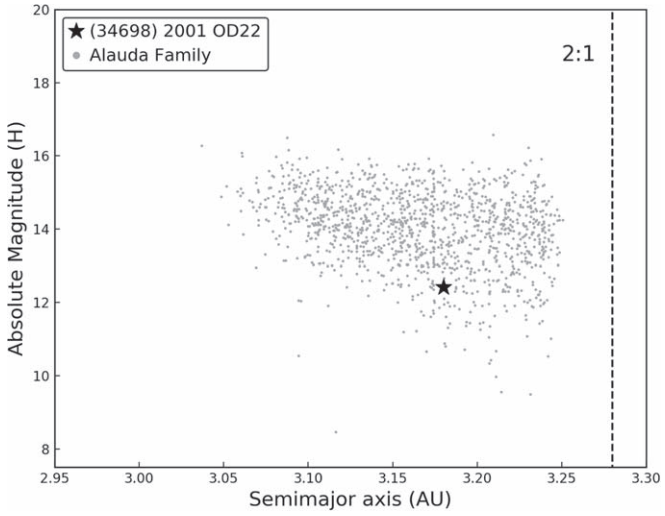

Figure 12. Absolute magnitude vs. semimajor axis for the Alauda family (Nesvorny 2015) and 2001 OD22. The location of the 2:1 mean motion resonance with Jupiter is depicted with a vertical dashed line.

The last condition that 2001 OD22 would have to meet to be considered a possible parent body for NWA 6704 is to be located close to a resonance capable of transporting fragments from this asteroid to near-Earth space. In order to investigate this in more detail, we have plotted the absolute magnitude as a function of semimajor axis for the Alauda family and 2001 OD22 (Figure 12). As can be seen in this figure, the "V" shape of the family is truncated at the 2:1 mean motion resonance with Jupiter ($a \approx 3.28$ au), an indication that asteroids from this family have been removed by this resonance. The question arises whether those objects entered the near-Earth space or were ejected from the Main Belt. To answer this question, we looked at the recent work of Granvik et al. (2018), who modeled the orbital evolution of near-Earth objects (NEOs) considering different escape regions in the Main Belt, including the 2:1 mean motion resonance. They found that only a small fraction of asteroids (∼4%) can escape from the 2:1 resonance to the near-Earth space, while the rest are ejected from the inner solar system. This suggests, that although possible, the probability for NWA 6704 to have originated in the Alauda family is low.

5. Conclusions

(1) Our goal was to find the parent asteroid of the anomalous achondrite NWA 6704. Curve-matching and taxonomic classification are unable to differentiate between Vesta-linked HED meteorites and anomalous achondrites in the VNIR wavelength range (0.35–2.5 μm).
(2) Similarly, we did not find any diagnostic absorption bands that would differentiate these meteorites in mid-IR wavelengths (2.5–25 μm); however, the strong principal Christiansen feature near 8.5 μm supports the pyroxene-dominated mineralogy.
(3) Spectral band parameters in the VNIR (Band I center, BAR) distinguish the anomalous achondrites from HED meteorites. NWA 6704 falls in the S(VI) of the Gaffey et al. (1993) S-asteroid subtype plot, whereas HED meteorites fall into the BA region.
(4) A search for the parent body of NWA 6704 should focus on V-type asteroids not dynamically linked to Vesta that fall in the S(VI) subtype of the Band I center versus BAR diagram.
(5) We investigated the V-type Main Belt asteroid (34698) 2001 OD22, a member of the Alauda family located close to the 2:1 resonance, as a potential parent source. However, given the difference in pyroxene chemistry between the asteroid and NWA 6704, and the small contribution of asteroids from this region to the NEO population, the probability for this asteroid to be the parent body is low.

This work was supported by NASA Planetary Missions and Data Analysis Program grant NNX14AN16G (PI: Le Corre) and state of Arizona Technology Research Initiative Fund (PI: Reddy). Appreciations to the cross-laboratorial assistance between Okayama University-Misasa, the Department of Geography at Winnipeg University, Planetary Science Institute, and the Lunar & Planetary Laboratory at The University of Arizona. A special thanks to those who provided comments and suggestions throughout the writing process, and to The University of Arizona's Writing Skills Improvement Program. Thank you to the reviewer's helpful comments in preparation of this manuscript for publication.

ORCID iDs

Vishnu Reddy https://orcid.org/0000-0002-7743-3491
Matthew R. M. Izawa https://orcid.org/0000-0001-5456-2912
Lucille Le Corre https://orcid.org/0000-0003-0349-7932
Edward A. Cloutis https://orcid.org/0000-0001-7301-0929

References

Adams, J. B. 1974, JGR, 79, 4829
Altomare, A., Corriero, N., Cuocci, C., et al. 2015, JApCr, 48, 598
Amelin, Y., Koefoed, P., Iizuka, T., et al. 2019, GeCoA, 245, 628
Archer, G. J. 2017, PhD Dissertation, Univ. Maryland
Benedix, G. K., Bland, P. A., Friedrich, J. M., et al. 2017, GeCoA, 208, 145
Binzel, R. P., & Xu, S. 1993, Sci, 260, 186
Bish, D. L., & Post, J. E. 1993, AmMin, 78, 932
Bland, P. A., Spurny, P., Towner, M. C., et al. 2009, Sci, 325, 1525
Burbine, T. H., Buchanan, P. C., Klima, R. L., & Binzel, R. P. 2018, JGRE, 123, 1791
Clark, R. N., & Roush, T. L. 1984, JGR, 89, 6329
Clayton, R. N. 1993, AREPS, 21, 115
Clayton, R. N., & Mayeda, T. K. 1996, GeCoA, 60, 1999
Clayton, R. N., & Mayeda, T. K. 1999, GeCoA, 63, 2089
Clayton, R. N., Onuma, N., & Mayeda, T. K. 1976, E&PSL, 30, 10
Cloutis, E. A. 2002, JGRE, 107, 5039
Cloutis, E. A., Berg, B., Mann, P., & Applin, D. 2016, Icar, 264, 20
Cloutis, E. A., & Gaffey, M. J. 1991, JGR, 96, 809
Cloutis, E. A., Gaffey, M. J., Jackowski, T. L., & Reed, K. L. 1986, JGR, 91, 641
Cloutis, E. A., Mann, P., Izawa, M. R. M., et al. 2013, Icar, 225, 581
Cooper, B. L., Salisbury, J. W., Killen, R. M., & Potter, A. E. 2002, JGRE, 107, 5017
DeMeo, F. E., Binzel, R. P., Slivan, S. M., & Bus, S. J. 2009, Icar, 202, 160
Drake, M. J. 1979, in Asteroids, ed. T. Gehrels (Tucson, AZ: Univ. Arizona Press), 765
Fernandes, V. A., Burgess, R., Crowther, S. A., et al. 2013, LPI, 44, 1719
Fitz Gerald, J. D., Parise, J. B., & Mackinnon, I. D. R. 1986, AmMin, 71, 1399
Fleet, M. E. 1977, AmMin, 62, 341
Gaffey, M. J. 1976, JGR, 81, 905
Gaffey, M. J. 1997, Icar, 127, 130
Gaffey, M. J., Bell, J. F., Brown, R. H., et al. 1993, Icar, 106, 573
Garvie, L. A. J. 2012, Catalogue of Meteorites from South America. The Meteoritical Bulletin, No. 99.https://www.lpi.usra.edu/meteor/docs/mb99.pdf
Gil-Hutton, R. 2006, Icar, 183, 93

Granvik, M., Morbidelli, A., Jedicke, R., et al. 2018, Icar, 312, 181
Grazulis, S., Chateigner, D., Downs, R. T., et al. 2009, JApCr, 42, 726
Greenwood, R. C., Barrat, J.-A., Scott, E. R. D., et al. 2013, LPI, 44, 3048
Greenwood, R. C., Burbine, T. H., Miller, M. F., & Franchi, I. A. 2017, ChEG, 77, 1
Greenwood, R. C., Franchi, I. A., Jambon, A., & Buchanan, P. C. 2005, Natur, 435, 916
Gualtieri, A. F. 2000, JApCr, 33, 267
Hall, S. R., & Stewart, J. M. 1973, Can. Mineral., 12, 169
Hardersen, P. S., Gaffey, M. J., & Abell, P. A. 2004, Icar, 167, 170
Hardersen, P. S., Reddy, V., Cloutis, E., et al. 2018, AJ, 156, 11
Harloff, J., & Arnold, G. 2001, P&SS, 49, 191
Hibiya, Y., Archer, G. J., Tanaka, R., et al. 2019, GeCoA, 245, 597
Hinrichs, J. L., & Lucey, P. G. 2002, Icar, 155, 169
Hugh-Jones, D. A., & Angel, R. J. 1994, AmMin, 79, 405
Iizuka, T., Amelin, Y., Puchtel, I. S., et al. 2013, LPI, 44, 1841
Irving, A. J., & Kuehner, S. M. 2011, Meteorite Classification (Seattle, WA: Univ. Washington)
Irving, A. J., Tanaka, R., Steele, A., et al. 2011, M&PSA, 74, 5231
Jambon, A., Humayun, M., & Barrat, J. A. 2012, LPSC, 43, 2099
King, T. V. V., & Ridley, I. W. 1987, JGR, 92, 11457
Klima, R. L., Dyar, M. D., & Pieters, C. M. 2011, M&PS, 46, 379
Klima, R. L., Pieters, C. M., & Dyar, M. D. 2007, M&PS, 42, 235
Klima, R. L., Pieters, C. M., & Dyar, M. D. 2008, M&PS, 43, 1591
Koefoed, P. P. 2017, PhD thesis, Australian National Univ.
Larsen, H. P., & Fink, U. 1975, Icar, 26, 420
Lazzaro, D., Michtcheno, T., Carvano, J. M., et al. 2000, Sci, 16, 2033
Leith, T. B., Moskovitz, N. A., Mayne, R. G., et al. 2017, Icar, 295, 61
Lenaz, D., Skogby, H., Princivalle, F., & Halenius, U. 2004, PCM, 31, 633
Le Corre, L., Reddy, V., Sanchez, J. A., et al. 2015, Icar, 258, 483
Lucas, M. P., Emery, J. P., Hiroi, T., & McSween, H. Y. 2019, M&PS, 54, 157
Mayne, R. G., McSween, H. Y., Jr., McCoy, T. J., & Gale, A. 2009, GeCoA, 73, 794
McCord, T. B., Adams, J. B., & Johnson, T. V. 1970, Sci, 168, 1445
McFadden, L. A., & Cline, T. P. 2005, M&PS, 40, 151
McSween, H. Y., Binzel, R. P., De Sanctis, M. C., et al. 2013, M&PS, 48, 2090
Migliorini, A., De Sanctis, M. C., Lazzaro, D., & Ammannito, E. 2017, MNRAS, 464, 1718
Morimoto, N., & Güven, N. 1970, AmMin, 55, 1195
Moroz, L., Schade, U., & Wasch, R. 2000, Icar, 147, 79
Nafziger, R. H., & Muan, A. 1967, AmMin, 52, 1364
Nash, D. B., & Conel, J. E. 1974, JGR, 79, 1615
Nesvorny, D. 2015, PDSS, 234, 0
Novakovic, B., Cellino, A., & Knežević, Z. 2011, Icar, 216, 69
Olsen, M. B., Wielandt, D., Schiller, M., Van Kooten, E. M. M. E., & Bizzarro, M. 2016, GeCoA, 191, 118
Pecharsky, V. K., & Zavalij, P. Y. 2005, Fundamentals of Powder Diffraction and Structural Characterization of Materials (New York: Springer)
Pompilio, L., Pedrazzi, G., Sgavetti, M., et al. 2009, Icar, 201, 781
Pompilio, L., Sgavetti, M., & Pedrazzi, G. 2007, JGR, 112, E01004
Reddy, V., Dunn, T. L., Thomas, C. A., Moskovitz, N. A., & Burbine, T. H. 2015, in Asteroids IV, ed. P. Michel, F. E. DeMeo, & W. F. Bottke (Tucson, AZ: Univ. Arizona Press), 43
Reddy, V., Sanchez, J. A., Nathues, A., et al. 2012, Icar, 217, 153
Rietveld, H. M. 1969, JApCr, 2, 65
Rojo, P., & Margot, J. L. 2007, CBET, 1016, 1
Rojo, P., & Margot, J. L. 2011, ApJ, 727, 69
Salisbury, J. W., Walter, L. W., & Vergo, N. 1987, Mid-Infrared (2.1–25 μm) Spectra of Minerals: First Edition, U.S. Geological Survey Open File Rep. 87
Sanborn, M. E., Wimpenny, J., Williams, C. D., et al. 2019, GeCoA, 245, 577
Sanchez, J. A., Reddy, V., Nathues, A., et al. 2012, Icar, 220, 36
Scott, E. R. D., Greenwood, R. C., Franchi, I. A., & Sanders, I. S. 2009, GeCoA, 73, 5835
Shankland, K. 2004, NISTJ, 109, 143
Smyth, J. R., & Hazen, R. M. 1973, AmMin, 58, 588
Sunshine, J. M., Bus, S. J., McCoy, T. J., et al. 2004, M&PS, 39, 1343
Sunshine, J. M., & Pieters, C. M. 1998, JGR, 103, 675
Thompson, S. P., Parker, J. E., Potter, J., et al. 2009, RScI, 80, 075107
Warren, P. H. 2011, E&PSL, 311, 93
Warren, P. H., Rubin, A. E., Isa, J., et al. 2013, GeCoA, 107, 135
Weichert, U. H., Halliday, A. N., Palme, H., & Rumble, D. 2004, E&PSL, 221, 373
Weisberg, M. K., McCoy, T. J., & Krot, A. N. 2006, in Meteorites and the Early Solar System II, ed. D. S. Lauretta & H. Y. McSween, Jr (Tucson, AZ: Univ. Arizona Press), 19
Wilburn, D. R., & Bassett, W. A. 1978, AmMin, 63, 591
Wilson, S. A., Raudsepp, M., & Dipple, G. M. 2006, AmMin, 91, 1331
Wood, B. J. 1974, AmMin, 5, 244
Yamaguchi, A., Clayton, R. N., Mayeda, T. K., et al. 2002, Sci, 296, 334
Young, R. A. 1993, in The Rietveld Method, ed. R. A. Young (Oxford: Oxford Univ. Press), 1
Young, R. A., Mackie, P. E., & Von Dreele, R. B. 1977, JApCr, 10, 262